Supplement of:

Soil processes govern alkalinity and cation retention in enhanced weathering for carbon dioxide removal

Jens S. Hammes¹, Jens Hartmann², Johannes A. C. Barth³, Tobias Linke², Ingrid Smet¹, Mathilde Hagens⁴, Philip A.E. Pogge von Strandmann⁵, Tom Reershemius⁶, Bruno Casimiro⁶, Arthur Vienne⁷, Anna A. Stoeckel¹, Ralf Steffens¹, Dirk Paessler¹

⁴ Soil Chemistry Group, Wageningen University & Research, Wageningen, 6700, Netherlands.

Correspondence to: Jens S. Hammes (jens.hammes@carbon-drawdown.de)

¹ Carbon Drawdown Initiative, Fürth, 90766, Germany.

² Department of Earth System Sciences, Universität Hamburg, Hamburg, 20146, Germany.

³ Department of Geography and Geosciences, GeoZentrum Nordbayern, Friedrich-Alexander- Universität Erlangen-Nürnberg (FAU), Erlangen, 91054, Germany.

⁵ MIGHTY (Mainz Isotope and Geochemistry Centre), Institute of Earth Sciences, Johannes Gutenberg University, Mainz, 55099, Germany.

⁶ School of Natural and Environmental Sciences, Newcastle University, Newcastle-upon-Tyne, NE1 7RU, UK.

⁷ Biobased Sustainability Engineering (SUSTAIN), Department of Bioscience Engineering, University of Antwerp, Antwerp, 2020, Belgium.

20 Supplementary material:

Table S1. Physicochemical parameters of the reference soils from Fürth and LUFA (versions 2.1, 2.2, and 6S) analyzed in this study.

pH: Soil pH was measured potentiometrically in 0.01 M CaCl₂ at a 1:2.5 soil:solution ratio (5 g <2 mm soil + 12.5 mL CaCl₂). Slurries were shaken, left to equilibrate for 1 h to settle, and the pH was recorded.) Effective CEC: CECeff was determined by extraction with unbuffered 1.0 M NH₄Cl. Fine soil (5 g) was combined with 50 mL extractant in 100 mL PE bottles, shaken, and equilibrated ≥12 h. Supernatant pH was recorded, and exchangeable Ca²+, Mg²+, K+, Na+, Al³+, Fe³+, and Mn²+ were measured by ICP-OES. The NH₄Cl stock had pH 4.88 (EC = 112.5 mS cm⁻¹); because post-equilibration pH (5.61–6.91) exceeded the stock pH, exchangeable H+ was not measured separately. total organic and inorganic carbon: TOC and TIC measured with a EA1108 Elemental Analyzer. grain size distribution: Particle-size distribution (fine fraction <2 mm) was measured to classify soil texture. Air-dried soil (10 g) was dispersed in 200 mL deionized water + 80 mL 0.1% Na₄P₂O₇·10H₂O (500 mL PE bottle) and shaken for 16 h. Sand was separated by wet sieving through a pre-dried, pre-weighed stack (630, 200, 63 µm). The <63 µm fraction (silt + clay) was collected, bottles/sieves rinsed, and the suspension concentrated at 80 °C to ~80 mL, then analyzed by Sedigraph (X-ray attenuation) to quantify silt and clay. major oxides, heavy metals and loss on ignition (LOI): major oxides and heavy metals were measured with a XRF. The LOI was determined by heating the sample at 1000 °C for 2 hours.

Unit	Parameter	Fürth 1	Fürth 2	LUFA 2.1	LUFA 2.2 A (2023)	LUFA 2.2 B (2024)	LUFA 6S A (2023)	LUFA 6S B (2024)		
	USDA Classification	loamy sand	loamy sand	sand	sandy loam	sandy loam	clay	clay		
	KA6 soil classification (German standard)	Strongly loamy sand	Moderately loamy sand	Sand	Moderate loamy sand	Strongly loamy sand	clay loam	Loamy clay		
	KA6 code	SI4	SI3	Ss	SI3	SI4	Lt3	TI		
	pН	7.10	7.15	4.60	5.50	5.61	7.30	7.31		
meq/100g	CEC (eff)	10.70	10.20	2.90	8.50	9.46	18.70	19.09		
wt%	тос	1.08	0.97	1.28	1.94	1.97	1.46	2.05		
wt%	TIC	0.15	0.14	BDL	BDL	0.01	0.26	0.37		
			Grain size d	istribution	1					
μm	Mean	163.75	149.24	194.49	167.40	190.90	27.02	59.89		
μm	d10	8.20	7.09	42.33	37.76	35.88	2.43	3.11		
μm	d50	129.75	118.60	179.41	153.79	177.97	9.13	22.36		
μm	d60	182.10	164.88	212.66	182.34	210.24	13.62	34.74		
μm	d90	376.97	343.52	365.05	314.21	357.41	90.12	191.34		
			Major Oxide	s and LOI						
wt%	SiO2	79.54	81.44	88.04	83.51	83.55	61.53	58.23		
wt%	A/2O3	7.48	7.27	3.54	5.27	5.13	11.44	12.21		
wt%	Fe2O3	2.04	2.02	1.75	2.02	1.18	4.90	4.85		
wt%	MnO	0.11	0.11	0.03	0.04	0.03	0.11	0.11		
wt%	MgO	0.41	0.37	0.10	0.21	0.19	3.27	3.81		
wt%	CaO	0.62	0.51	0.19	0.37	0.40	1.75	2.17		
wt%	Na2O	0.49	0.49	0.39	0.42	0.34	0.46	0.37		
wt%	K20	3.99	3.96	1.88	2.01	1.96	3.71	3.98		
wt%	P2O5	0.21	0.20	0.08	0.10	0.11	0.21	0.22		
wt%	TiO2	0.24	0.23	0.14	0.25	0.25	0.58	0.61		
wt%	LOI	3.90	3.39	2.83	5.50	5.95	11.41	13.40		
Heavy metals										
ppm	Cr	68	68	< 68	< 68	< 68	68	< 68		
	Co	< 37	< 37	< 37	< 37	< 37	< 37	< 37		

Table S2. Mineralogical composition (wt%) of the main 7 used feedstocks (6 rocks and 1 industrial material) as well as the 7 EW suppliers' feedstocks, analyzed in this study by quantitative XRD. serp. = serpentinised.

Theoretical	Mineral	serp.	leucite basanite	calcite rich meta-	dolomitic limestone	glacial rock	steel slag	EW 1	EW 2 leuco-	EW 3 leuco-	EW 4 serp.	EW 5 serp.	EW 6 serpenti	EW 7
formula	name	•		basalt		flour		concrete	basalt	basalt	peridotite	peridotite		-basalt
SILICA	TES													
SiO ₂	Quartz			4.3	1.1	11.5		16.9	6.2	2.4	0.7	0.7	0.9	2.7
SiO ₂	Cristobalite													2.0
SiO ₂	Tridymite													1.9
KAISi₃O₃	K-feldspar			10.1		6.6		0.4	5.5					13.7
(Na,Ca)(Si,Al)₄O ₈	Plagioclase		7.7	15.5		35.3		1.7	33.8	58.6	1.2	0.7	1.2	38.1
(Ca,Na)(Mg,Fe,Al,Ti) (Si,Al)₂O ₆	Clinopyroxene	1.6	49.4	1.8		0.8			17.4	10.9	0.6	0.9	0.5	20.6
(Ca,Na)(Mg,Fe,Al,Ti) (Si,Al) ₂ O ₆	Orthopyroxene	5.0							3.5	7.0	3.1	3.4		3.7
Ca₂(Mg,Fe)₅Si₅O₂₂(O H)₂	Amphibole	1.9				14.1			1.5		2.2	0.7	0.5	
(Mg,Fe)₂SiO₄	Olivine	79.2	11.2	3.6					1.3	6.1	60.8	81.6	1.1	1.2
(Na,K)AlSiO₄	Nepheline		9.3								0.5			1.3
Na ₈ Al ₆ Si ₆ O ₂₄ Cl ₂	Sodalite		0.5											
KAISi ₂ O ₆	Leucite	0.3	12.6											
NaAlSi ₂ O ₆ •(H ₂ O)	Analcime		1.3											
α-Ca ₂ (SiO ₄)(H ₂ O)	Alpha-Dicalcium Silicate hydrate						6.2							
Ca₂SiO₄	Beta C2S* (Lamite)						8.9							0.4
Ca₂SiO₄	Alpha' C2S						14.8							
(K,H ₂ O)(Al,Mg,Fe) ₂ (Si,Al) ₄ O ₁₀ [(OH) ₂ ,(H ₂ O)]	2:1 layer silicates	0.5	1.8	6.2	0.1	28.5		2.5	23.3	12.1	0.6			6.1
(Mg,Fe)₅Al(Si₃Al)O₃₀(OH)₃	Chiorite	1.4		22.5		1.4		0.3	1.2	1.3	4.4		2.3	
X ₃ Z ₂ (SiO ₄) ₃	Garnet						4.5							
Al ₂ Si ₂ O ₅ (OH) ₄	Kaolinite								0.7		2.7	8.0	0.7	
(Mg,Fe,Ni,Mn,Al,Zn) ₃	Serpentine	10.3									16.8	9.1	84.1	

[Si ₂ O ₅](OH) ₄													
Mg ₃ Si ₄ O ₁₀ (OH) ₂	Talc								0.3	4.7	0.8		
CaTiSiO₅	Titanite		6.5										
CARBOI	NATES												
CaCO₃	Calcite		27.2	85.0	0.6	8.3						0.5	61.2
CaCO₃	Aragonite											0.6	
Ca(Fe ²⁺ x,	Dolomite/Ankerit			40.7	0.5		0.0		0.0	0.0	0.0		0.0
Mg _{1-X})(CO ₃) ₂	е			13.7	0.5		9.3		0.6	0.3	0.2		0.9
Mg ₆ Al ₂ (CO ₃)(OH) ₁₆ •4 (H ₂ O)	Hydrotalcite						0.5			0.5	0.3	0.6	
Na ₂ CO ₃	Natrite						1.7						
PHOSPI	HATES												
Cas(PO ₄) ₃ (OH,F,CI)	Apatite	1.2	0.8				0.9	0.5					1.5
SULPH	IATES												
CaSO₄•2(H₂O)	Gypsum						0.9						
Ca ₆ Al ₂ (SO ₄) ₃ (OH) ₁₂ •2 6(H ₂ O)	Ettringite/Aft**						0.9						
HALI	DES												
NaCl	Halite				0.7		0.2						
OXIDES/HYI	DROXIDES												
TiO ₂	Anatase		0.8										
Fe₂O₃	Hematite		0.7	0.1				0.2					
Fe ²⁺ Fe ³⁺ ₂ O ₄	Spinel-type minerals	4.8				5.9		2.8	0.4	0.4	0.8	5.1	2.1
Fe²+TiO₃	Ilmenite							2.1	0.3	0.3			4.4
FeO	Wuestite					10.8							
CaO	Lime					1.9							
Ca(OH)₂	Portlandite					19.5							
Mg(OH)₂	Brucite											1.9	
MgO	Periclase					0.7							
Ca₂Fe³+₂O₅	Srebrodolskite					17.8	0.3						
ELEME	ENTS												
Fe	Iron					0.7							

Table S3. Major oxide composition and heavy metal concentrations of the main used feedstocks (6 rocks and 1 industrial material) and 7 EW company feedstocks analysed by XRF. Loss on Ignition (LOI) was determined through heating at 1000 degrees C for 2 hours; serp. = serpentinised.

			serp. peridotite	leucite basanite	calcite rich meta-basalt	dolomitic limestone	glacial rock flour	steel slag	EW 1 cement concrete	EW 2 leuco- basalt	EW 3 leuco- basalt	EW 4 serp.	EW 5 serp. peridotite	EW 6 serpenti- nite	EW 7 leuco -basalt
Detection limit	Unit	Element													
0.01	%	SiO2	41.08	43.3	34.7	1.37	54.52	10.79	18.53	49.73	47.93	41.73	41.56	33.83	49.6 2
0.01	%	Al2O3	0.53	13.4	11.52	0.63	16.11	2.85	1.93	13.3	18.79	0.84	0.42	1.9	12.3 8
0.01	%	Fe2O3	7.15	10.95	11.12	0.4	8.21	23.85	1.11	13.4	8.31	6.92	8.49	7.58	15.1 5
0.005	%	MnO	0.102	0.185	0.148	0.046	0.118	1.62	0.05	0.189	0.127	0.095	0.118	0.106	0.20 7
0.01	%	MgO	47.27	9.8	5.09	3.27	4.8	4.85	2.81	5.74	8.38	45.76	47.49	34.73	4.04
0.01	%	CaO	0.24	12.7	16.09	51.64	3.82	43.12	40.86	8.18	10.87	0.23	0.3	1.06	7.9
0.01	%	Na2O	0.03	2.63	1.96	<0.01	3.97	0.03	0.11	2.67	2.19	0.11	0.1	0.07	2.64
0.01	%	K20	0.03	3.08	2.03	0.13	3.46	< 0.01	0.3	1.41	0.37	0.08	0.03	0.03	1.55
0.01	%	TiO2	0.01	2.73	3.54	0.02	0.68	0.53	0.1	2.35	0.36	0.01	0.03	0.04	3.72
0.01	%	P2O5	0.01	0.55	0.48	0.01	0.12	1.42	0.04	0.28	0.12	< 0.01	0.01	< 0.01	0.47
0.01	%	LOI	1.57	0.6	13.21	43.23	4.84	10.68	34.4	3.14	3.06	3.82	1	15.08	1.69
68	ppm	Cr	1778	205	68	<68	205.2	1300	< 68	137	342	2463	3216	29352	< 68
37	ppm	Co	110	51	59	<37	44.04	<37	< 37	44	44	104	126	96	44
40	ppm	Cu	<40	80	48	<40	55.93	<40	< 40	40	88	< 40	< 40	< 40	40
24	ppm	Ni	2687	118	110	<24	149.34	<24	< 24	39	157	2601	2915	2263	< 24
17	ppm	V	<17	286	129	<17	106.4	1703	39	336	106	< 17	< 17	90	403

Table S4. Particle size distribution (measured by dispersion in water with laser diffraction; results are shown as mean, mode, and percentile values d10, d50, d60, d90) and specific surface area (BET measured with a Quantachrome Autosorb using N_2 as adsorptive-gas) of the 7 main used feedstocks (6 rock and 1 industrial material) and 7 EW company feedstocks analysed in this study. serp. = serpentinised

Unit	Parameter	serp. peridotite	leucite basanite	calcite rich metabasalt		glacial rock flour	steel slag	EW 1 cement concrete	EW 2 leuco- basalt	EW 3 leuco- basalt	EW 4 serp. peridotite	EW 5 serp. peridotite	EW 6 serpentinite	EW 7 leuco -basalt
	PARTICLE SIZE DISTRIBUTION													
μm	Mean	23.9	152.7	17.2	193.47	1.9	82.5	285.5	128.7	36.5	21.2	17.5	118.19	130.8
μm	Standard Deviation	18.5	188.5	16.3	132.82	1.3	61.6	251.1	130.1	41.5	16.2	13.2	115.21	129.2
μm	Mode	34.2	401.2	27.6	255.25	2.4	111	454.6	244.9	53.3	26.4	23.4	207.7	235.04
μm	d10	4.1	3.9	2.4	5.74	0.4	6.1	18.2	4.5	3.2	4.1	3.4	6.51	10.9
μm	d50	19.6	38.5	11.2	203.44	1.6	76.4	233.8	77.8	20.6	17.5	14.5	80.27	85.0
μm	d60	25	68.1	17.1	233.81	2.0	93.4	319.6	149.5	29.9	22.1	18.5	115.11	122.8
μm	d90	50.6	447.5	41.2	361.29	3.8	167.2	643.5	319.1	93.3	44.3	36.4	289.73	322.8
	SPECIFIC SURFACE AREA													
m²/g	BET area	1.9	2.3	2.6	0.873	17.8	13.3	19.5	2.4	6.7	3.2	1.9	15.1	6.5

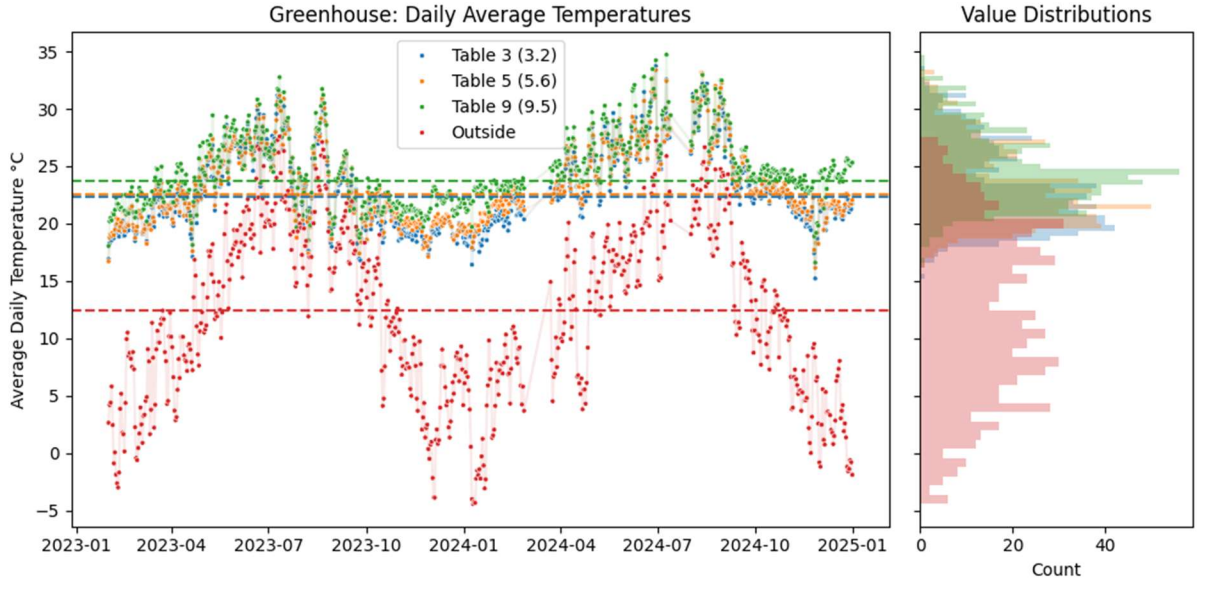


Figure S1. Daily average soil temperatures (blue, orange and green dots) monitored over two years in greenhouse experiments. Measurements were taken from soils in Table 3 (blue), Table 5 (orange), and Table 9 (green), which represent sampling points distributed throughout the greenhouse. Red dots represent the corresponding outside air temperature during the same period. Value distributions are shown on the right.

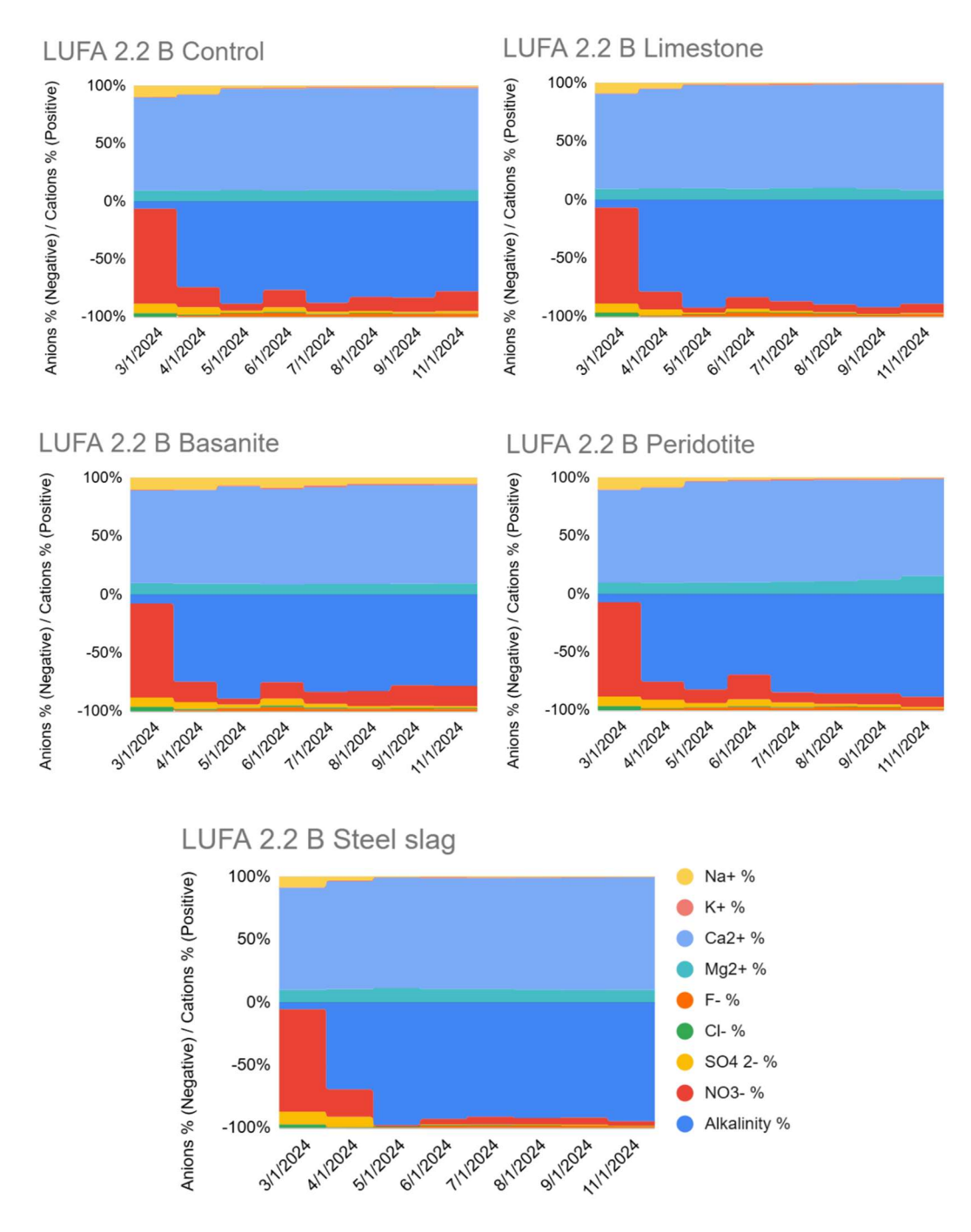


Figure S2. Monthly cation-anion diagrams of leachate composition for LUFA 2.2 B. Stacked charge-percent compositions of leachate ions by month (Jan–Sep, Nov 2024) for five treatments: Control, Limestone, Basanite, Peridotite, and Steel slag. Each panel shows cations (positive, upper half: Na^+ , K^+ , Ca^{2+} , Mg^{2+}) and anions (negative, lower half: F^- , CI^- , SO_4^{2-} , NO_3^- , and alkalinity as carbonate species) as fractions of total charge. The y-axis is % charge (anions negative; cations positive). October is omitted because anion data was unavailable.

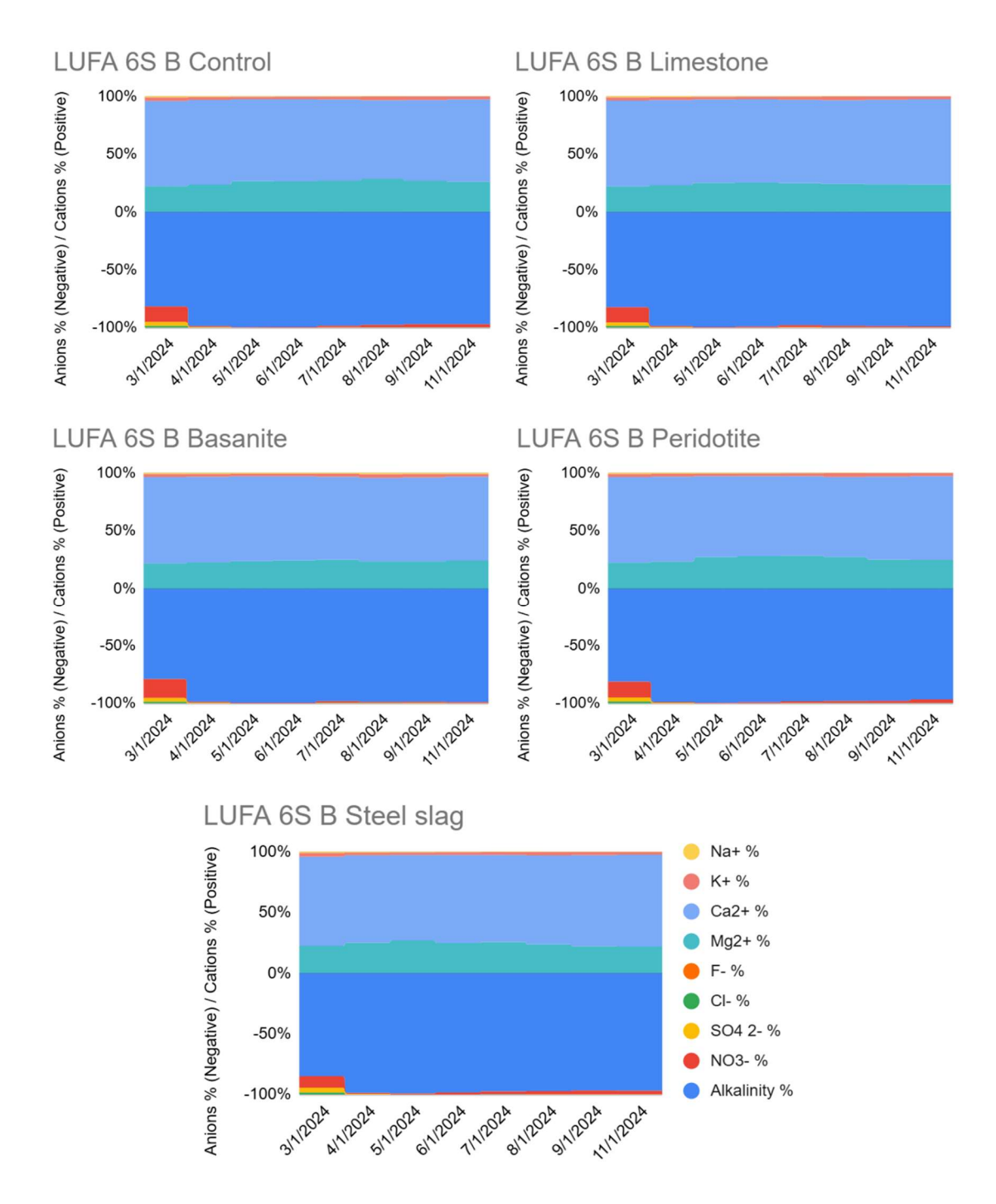


Figure S3. Monthly cation-anion diagrams of leachate composition for LUFA 6S B. Stacked charge-percent compositions of leachate ions by month (Jan-Sep, Nov 2024) for five treatments: Control, Limestone, Basanite, Peridotite, and Steel slag. Each panel shows cations (positive, upper half: Na⁺, K⁺, Ca²⁺, Mg²⁺) and anions (negative, lower half: F⁻, Cl⁻, SO₄²⁻, NO₅⁻, and alkalinity as carbonate species) as fractions of total charge. The y-axis is % charge (anions negative; cations positive). October is omitted because anion data was unavailable.

Greenhouse Experiment Fürth 2 soil

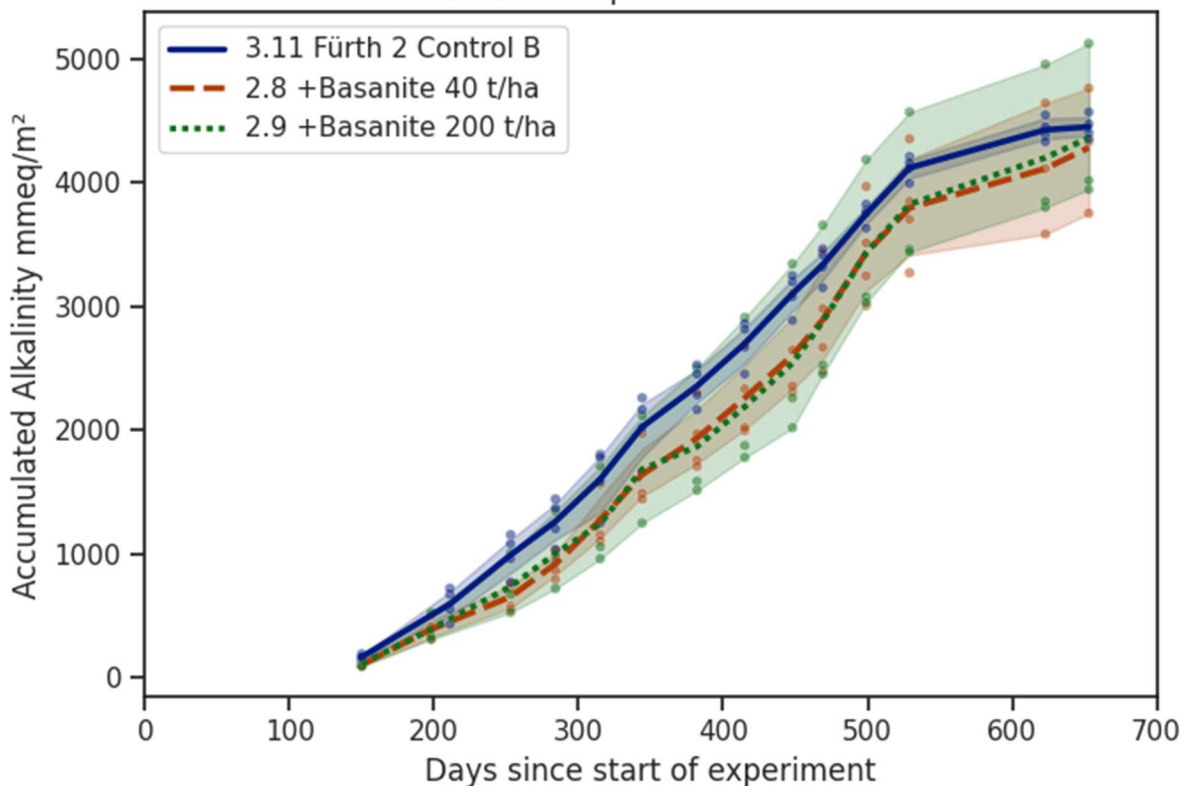


Figure S4: Accumulated leachate alkalinity results for Fürth 2 (n = 4 control and basanite 40 t ha^{-1} , n = 3 basanite 200 t ha^{-1}). The control treatment (blue) consists only of the second batch of 'Fürth' soil, while the other experiments included additions of basanite in 2 different application rates. Shaded areas represent the variability among replicates.

Table S5. Irrigation rates applied by period. Rates were adjusted over time to ensure adequate monthly leachate generation under periods of high evapotranspiration.

Time period	Irrigation rate
30.01.2023 - 20.05.2023	2000 mm a-1
20.05.2023 - 27.06.2023	3000 mm a-1
27.06.2023 - 08.08.2023	4000 mm a-1
08.08.2023 - 15.05.2024	2000 mm a-1
15.05.2024 - 03.06.2024	3000 mm a-1
03.06.2024 - 08.07.2024	2000 mm a-1
08.07.2024 - 29.08.2024	3000 mm a-1
29.08.2024 - 10.01.2024	2000 mm a-1

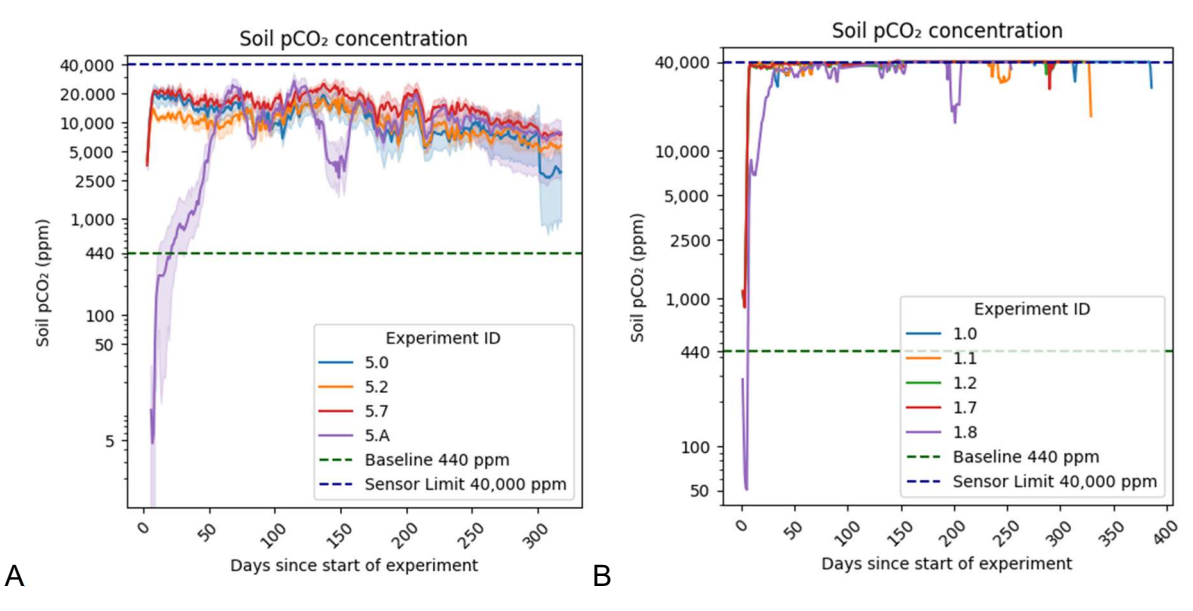
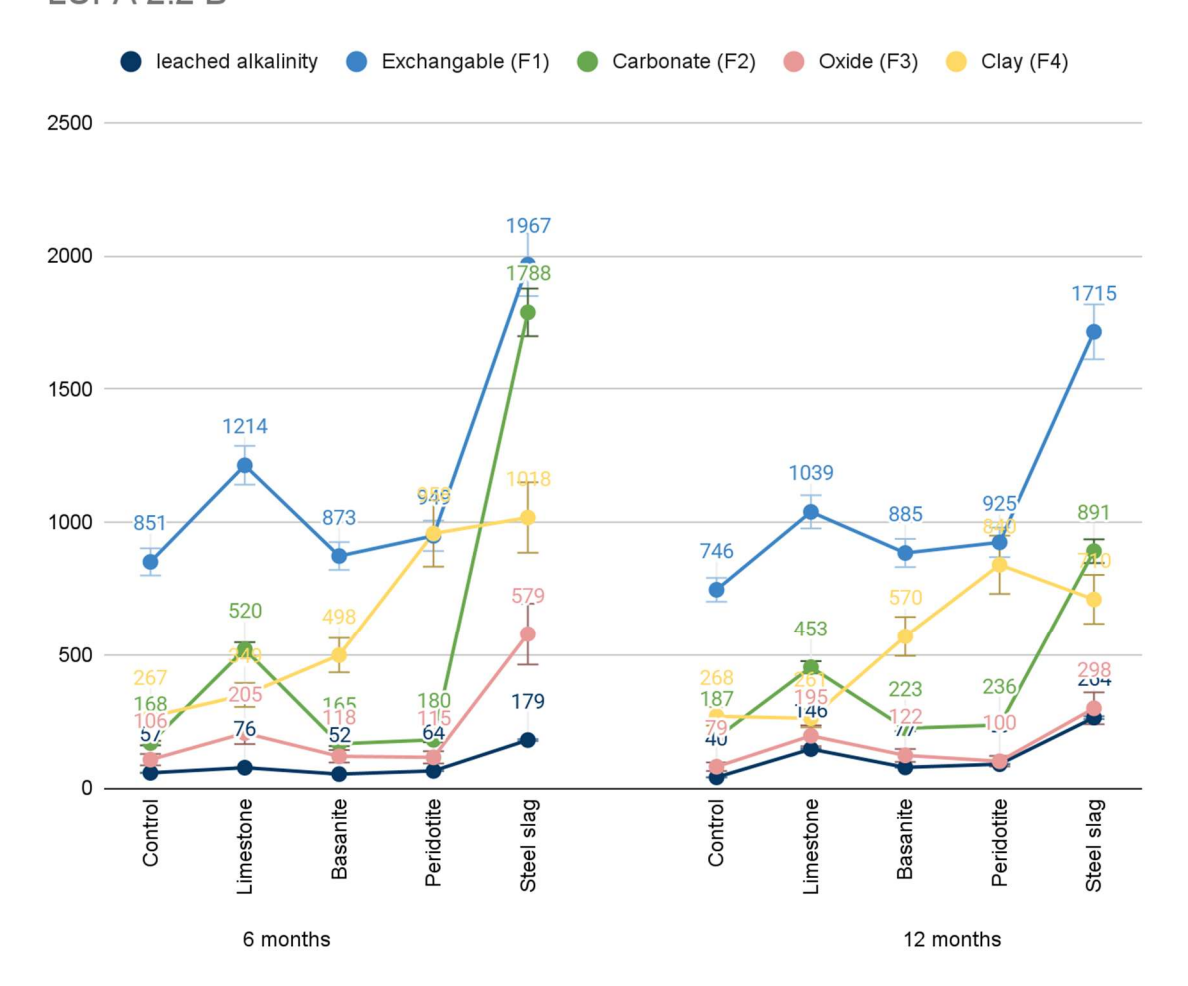


Figure S5 Soil pCO2 dynamics in LUFA 6S (log scale). Time series of measured soil pCO2 during the first 350 days after setup: (A) 'LUFA 6S A', initiated in 2023; (B) 'LUFA 6S B', initiated in 2024. The y-axis shows the CO2 concentration in ppm logarithmic. Dashed green line marks the atmospheric baseline (~440 ppm); dashed navy line marks the sensor upper limit (40,000 ppm). Days on the x-axis are counted from the start of each experiment.

LUFA 2.2 B



LUFA 6S B

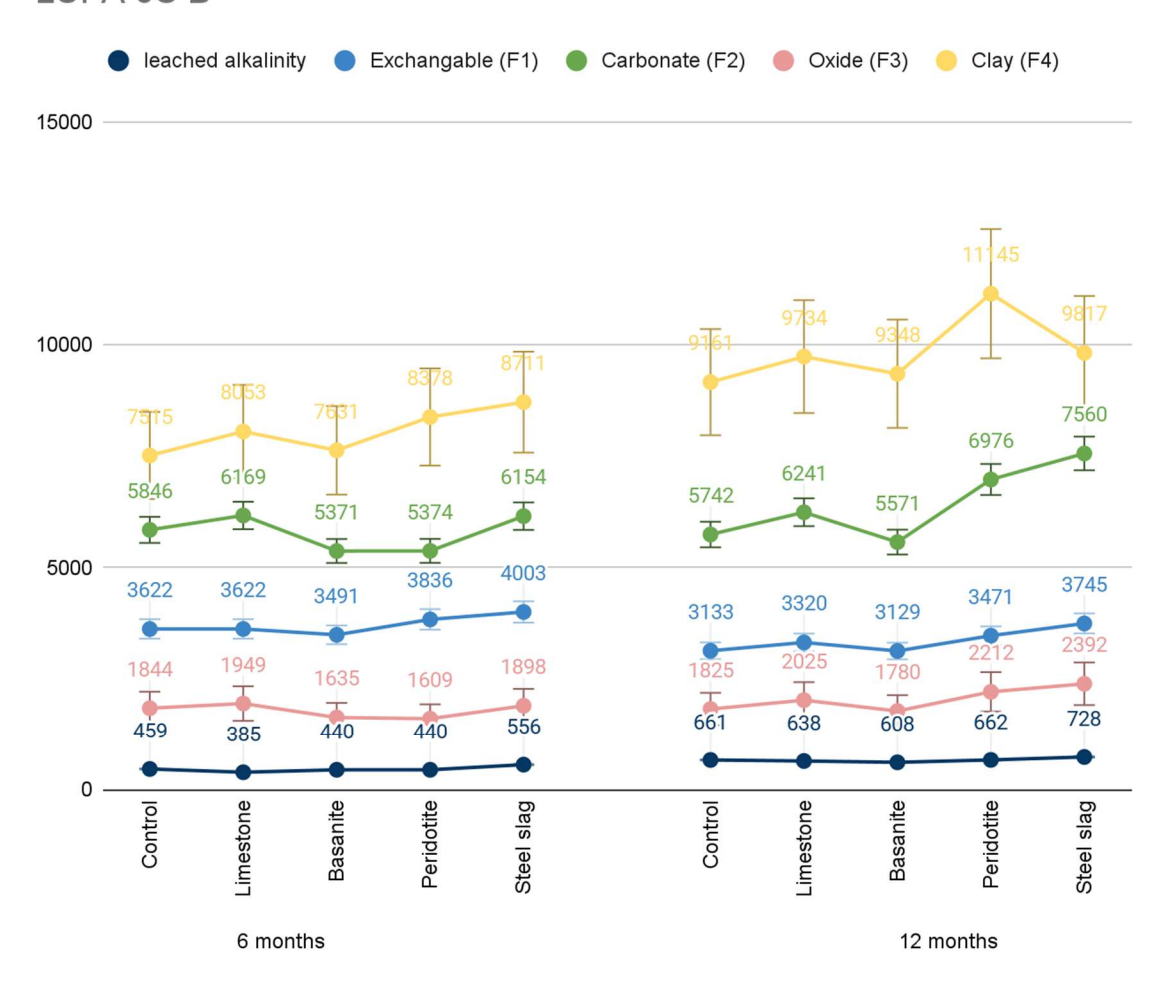
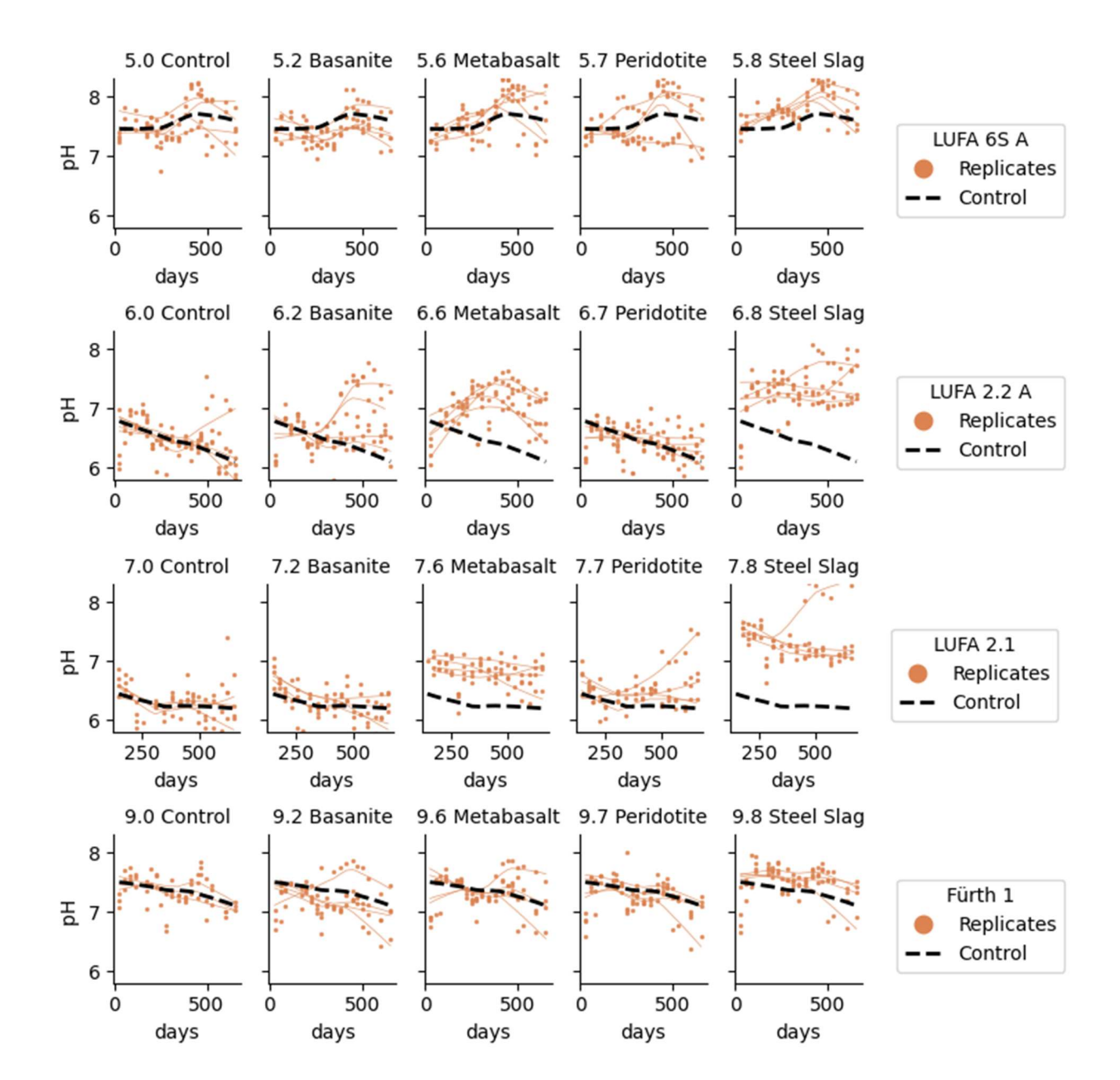


Figure S6. Cumulative leached alkalinity and potential alkalinity stored in solid-phase cation pools for the LUFA 2.2 B and LUFA 6S B experiments, shown by treatment and sampling duration. Categories on the x-axis are (left block) 6-month pots and (right block) 12-month pots; within each block the treatments are control, limestone, basanite, peridotite, and steel slag. The five plotted series are: leached alkalinity (meq pot⁻¹) and four sequential-extraction pools expressed as potential TA (meq pot⁻¹)—F1 Exchangeable, F2 Carbonate-associated, F3 Oxide (Fe/Mn oxide-bound), and F4 clays. 'Total potential TA' is defined as the sum of the charge equivalents of the major base cations Ca²⁺, Mg²⁺, Na⁺, and K⁺ contained in F1–F4; point labels give pool magnitudes (meq pot⁻¹). To estimate how much additional potential TA is attributable to a given amendment, compare each treatment to its contemporaneous control within the same time block. Controls are not subtracted in the plot; they are shown explicitly so readers can assess the absolute size and partitioning of pools across treatments and times, not only relative treatment–control deltas. A certified reference was analysed alongside all samples across four sequential fractions (F1–F4). Error bars representing the maximum observed fraction-specific σ (worst-case scenario) were added for visualisation purposes, acknowledging that typical uncertainties are smaller.



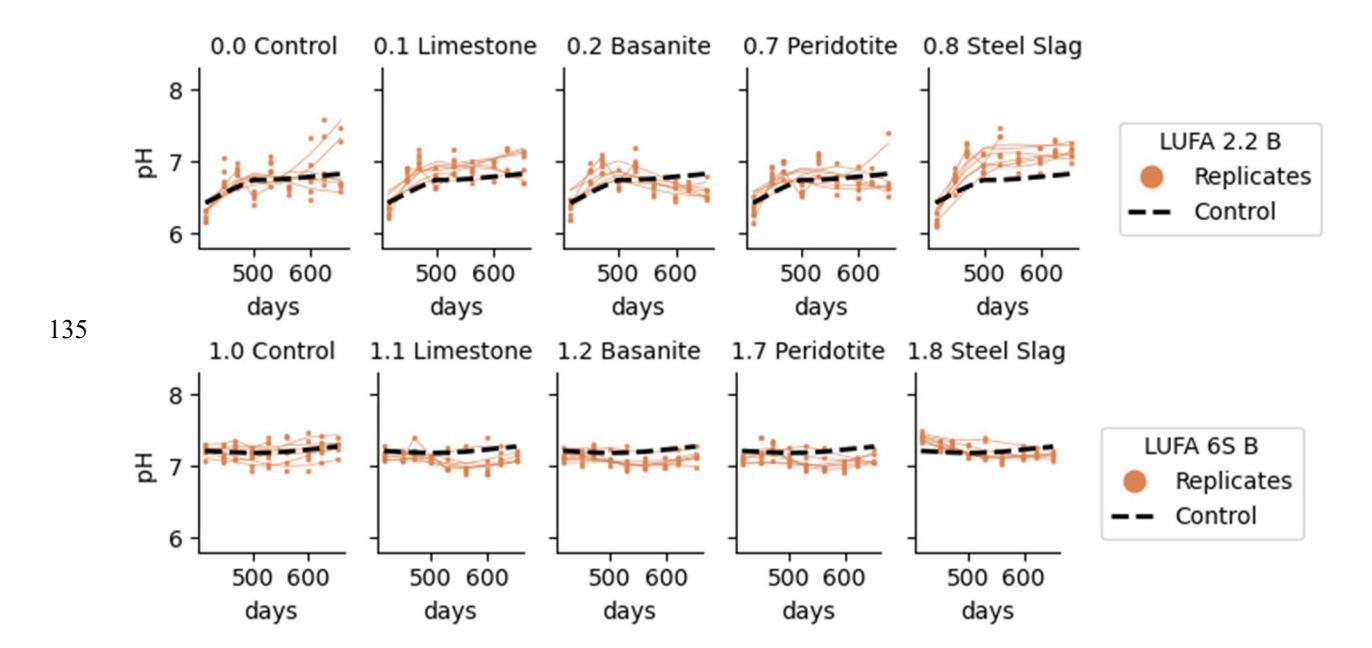


Figure S7. Leachate pH through time across soils and feedstocks. Time series of leachate pH for multiple soil-feedstock combinations. Each small panel shows one treatment (control, limestone, basanite, metabasalt, peridotite, or steel slag). Experiments started in 2023: LUFA 6S A, LUFA 2.2 A, LUFA 2.1, and Fürth 1, monitored for ~650 days. Experiments started in 2024: LUFA 2.2 B and LUFA 6S B, monitored for ~250 days (graphs start at 'day 400' for visualisation).

Supplementary chapter dissolution kinetics

140

145

Feedstocks reflect mineral dissolution kinetics

Whereas a feedstock's Ca, Mg, Na and K content indicates theoretically how much carbon it might sequester once it is completely weathered (Renforth, 2019), it is the type of minerals in which these major cations are present that influences how quickly the feedstock may dissolve and release alkalinity. Within the soil relevant pH range, many minerals tend to dissolve faster in low pH soils, explaining why the acidic soils LUFA 2.1, LUFA 2.2 A and LUFA 2.2 B generally lead to more alkalinity increase compared to the other more alkaline soils. Soil conditions thus strongly influence the minerals' reactivity and actual dissolution rates. However, at a given pH, it is the specific crystal structure and chemical bonds of the minerals that define their weathering rate.

The main feedstocks tested in this experiment represent 3 types of materials: alkaline industrial by-products (steel slag), carbonate (-rich) rocks (metabasalt and limestone) and silicate rocks (ultramafic peridotite and mafic basanite). Table S10 summarises the EW relevant minerals present in these feedstocks with estimations of their dissolution rate r at 25 °C and neutral pH (around 7). These data, gathered from Wang et al. (1998); Leineweber, (2002); Palandri & Kharaka (2004); Heřmanská et al. (2022; 2023), reflect faster dissolution at lower values. They are arranged from faster to slower dissolving minerals, with each unit of difference in -log Wr (for example from 8 to 9) representing an order of magnitude difference in

dissolution rates. As mineral dissolution rates change with temperature, pH, chemical environment as well as compositional variability of the minerals themselves, these data should not be used as absolute values but rather as a guideline to which minerals are relatively more easily weathered than others.

Table S6. Literature dissolution rate Wr at 25 °C and pH 7 for minerals relevant to enhanced weathering, reported as $-\log_{10}$ Wr (mol m⁻² s⁻¹), where lower values indicate faster dissolution. Sources: a = Wang et al. (1998); b = Leineweber (2002); c = Palandri & Kharaka (2004); d = Heřmanská et al. (2022; 2023).

160

Chemical formula	Mineral name	- Log ₁₀ Wr (mol/m ² s)	Mineral group (silicate mineral type)
Ca(OH) ₂	Portlandite	5.3a	Hydroxide
CaO	Lime	5.5 ^b	Oxide
CaCO ₃	Calcite	6.1 ^b	Carbonate
Ca ₂ SiO ₄	Larnite	6.3 ^d	(nesosilicate)
CaMg(CO ₃) ₂	Dolomite	7.0 ^b	Carbonate
(Na,K)AlSiO ₄	Nepheline	8.6°	Feldspathoid (Tectosilicate)
CaSiO ₃	Wollastonite	8.9°	(inosilicate)
KAlSi ₂ O ₆	Leucite	9.2°	Feldspathoid (tectosilicate)
Mg ₂ SiO ₄	Forsterite	9.5 ^d	Olivine (nesosilicate)
MgCaSi ₂ O ₆	Diopside	10.9 ^d	Clinopyroxene (inosilicate)
Not applicable	Basaltic glass	10.9 ^d	Amorphous silica
(Ca,Na)(Al,Si) ₄ O ₈	Anorthite, bytownite, andesine, oligoclase, albite	11.0 ^d	Plagioclase (tectosilicate)
MgSiO ₃	Enstatite	11.5 ^d	Orthopyroxene (inosilicate)
(Ca,Na)(Mg,Fe,Al, Ti)(Si,Al) ₂ O ₆	Augite	11.9 ^d	Clinopyroxene (inosilicate)
$Mg_3Si_2O_5(OH)_4$	Lizardite, chrysotile	11.9 ^d	Serpentine (phyllosilicate)
(Ca,Na) ₂ (Mg,Fe,Al) ₅ (Al,Si) ₈ O ₂₂ (OH) ₂	Hornblende	11.9 ^d	Amphibole (inosilicate)
K(Mg,Fe) ₃ (AlSi ₃ O ₁₀)(F,OH) ₂	Biotite	12.1 ^d	Mica (phyllosilicate)
KAlSi ₃ O ₈	Orthoclase	12.3 ^d	K-feldspar (tectosilicate)
(Mg,Fe) ₃ (Si,Al) ₄ O ₁₀ (OH) ₂ -(Mg,Fe) ₃ (OH) ₆	Clinochlore	12.6 ^d	Chlorite (phyllosilicate)
SiO ₂	Quartz	13.0 ^d	(tectosilicate)
Al ₂ Si ₂ O ₅ (OH) ₄	Kaolinite	14.0 ^d	Clay (phyllosilicate)

The mineral composition of our steel slag comprises approximately 20 % portlandite, 2 % lime, 8 % calcite, and 24 % larnite.

These minerals represent the four fastest dissolving minerals in this table, explaining why steel slag outperformed all other feedstocks on each soil type with regard to increasing leachate alkalinity. Oxides and hydroxides of Ca and Mg are generally

rapidly weathering minerals, especially under acidic conditions, with dissolution rates up to order(s) of magnitude higher than carbonate or silicate minerals.

The carbonate (-rich) rocks tested in this study represented comparable amounts of calcite addition to the soils: we added the equivalent of 40 t ha⁻¹ for the metabasalt with 27 % calcite and 10t/ha for the limestone which consists of 85 % calcite (and 14 % dolomite). Although somewhat slower weathering than oxides and hydroxides, carbonate minerals still dissolve orders of magnitude faster than most silicate minerals. This explains why the limestone treatment resulted in the second-highest accumulated alkalinity increase relative to control in both LUFA 2.2 B and LUFA 6S B experiments. As for the metabasalt, which in addition to 27 % calcite also contains 4 % olivine and 16 % plagioclase, it is likely that fast dissolution of its carbonate mineral content was responsible for the stronger increase in leachate alkalinity of acid soils, especially in the first year.

To estimate the weathering potential of silicate rocks, one can refer to the Goldich dissolution series which ranks primary silicate minerals by their relative stability at the Earth's surface (Goldich, 1938). It is basically the reverse of Bowen's reaction series (Bowen, 1922) which describes the crystallisation sequence of silicate minerals in a cooling magma. Minerals formed at higher temperatures and pressures (e.g., olivine) are thereby more easily weathered than those formed at lower temperatures and pressures (e.g. quartz) which are more resistant to weathering. Secondary minerals which are formed through the alteration of primary ones (e.g. serpentine, clays) are even more stable and less susceptible to dissolution.

Olivine was among the first silicate minerals suggested for EW (Schuiling & Krijgsman, 2006) as it has a relatively high dissolution rate whilst also being abundantly present across the world. The peridotite feedstock applied in our experiment consisted of 79 % olivine along with some slower weathering pyroxene (7 %) and serpentine (10 %). In comparison, the basanite contained lower amounts of olivine (11 %), about 22 % of feldspathoids (nepheline and leucite) which have dissolution rates similar to olivine, but more clinopyroxene (49 %). Overall, this basanite's mineral content suggests somewhat less weathering potential than the peridotite.

In our EW experiments, we observed that accumulated leachate alkalinity of peridotite treatments was either similar to, or higher than, basanite treatments. In both the acidic LUFA 2.1 and LUFA 2.2 A soils, 2-year accumulation resulted in significantly more leachate alkalinity for the peridotite than the basanite. Interestingly, replicating the same feedstock-soil combination in a one year experiment (LUFA 2.2 B) produced similar accumulated leachate alkalinities for peridotite and basanite, which was also observed halfway through the LUFA 2.2 A experiment. In more pH neutral soils (Fürth and LUFA 6S A and B), both silicate feedstocks generated statistically similar leachate alkalinity signals, even though peridotite was usually slightly higher than basanite.

References

170

185

190

Bowen, N. L.: The Reaction Principle in Petrogenesis, The Journal of Geology, 30, 177–198, https://doi.org/10.1086/622871, 1922.

Goldich, S. S.: A Study in Rock-Weathering, The Journal of Geology, 46, 17–58, https://doi.org/10.1086/624619, 1938.

- Heřmanská, M., Voigt, M. J., Marieni, C., Declercq, J., and Oelkers, E.: A comprehensive and consistent mineral dissolution rate database: Part II: Secondary silicate minerals, Chem. Geol., 636, 121632, 2023.
- Heřmanská, M., Voigt, M. J., Marieni, C., Declercq, J., and Oelkers, E. H.: A comprehensive and internally consistent mineral dissolution rate database: Part I: Primary silicate minerals and glasses, Chem. Geol., 597, 120807, 2022.
 - Leineweber, D.: Production of Calcium Magnesium Acetate (CMA) from Dilute Aqueous Solutions of Acetic Acid, 2002.
 - Palandri, J. L. and Kharaka, Y. K.: A compilation of rate parameters of water-mineral interaction kinetics for application to geochemical modeling, Open-File Report, U.S. Geological Survey, https://doi.org/10.3133/ofr20041068, 2004.
- Renforth, P.: The negative emission potential of alkaline materials, Nat Commun, 10, 1401, https://doi.org/10.1038/s41467-019-09475-5, 2019.
 - Schuiling, R. D. and Krijgsman, P.: Enhanced Weathering: An Effective and Cheap Tool to Sequester Co2, Climatic Change, 74, 349–354, https://doi.org/10.1007/s10584-005-3485-y, 2006.
 - Wang, J., Keener, T. C., Li, G., and Khang, S.-J.: THE DISSOLUTION RATE OF Ca(OH)₂ IN AQUEOUS SOLUTIONS,
- 210 Chemical Engineering Communications, 169, 167–184, https://doi.org/10.1080/00986449808912726, 1998.